Polymer Journal, Vol. 37, No. 5, pp. 368–375 (2005)

Effects of Hydrophobic Chain Length on the Micelles of Heptaoxyethylene Hexadecyl $C_{16}E_7$ and Octadecyl $C_{18}E_7$ Ethers

Yoshiyuki EINAGA,† Ai KUSUMOTO, and Akane NODA

Department of Chemistry, Nara Women's University, Kitauoya Nishi-machi, Nara 630-8506, Japan

(Received January 4, 2005; Accepted February 1, 2005; Published May 15, 2005)

ABSTRACT: Micelles of heptaoxyethylene hexadecyl $C_{16}E_7$ and octadecyl $C_{18}E_7$ ethers in dilute aqueous solutions were characterized at finite surfactant concentrations c by static (SLS) and dynamic light scattering (DLS) experiments at several temperatures T below the critical points, in order to examine the effects of hydrophobic chain length on size, shape, structure, etc., of the micelles. The SLS results were successfully analyzed by the thermodynamic theory formulated with wormlike spherocylinder model for SLS of micelle solutions, thereby yielding the molar mass M_w of the micelles as a function of c and the cross-sectional diameter d, indicating that the micelles assume a flexible spherocylindrical shape. The radius of gyration $\langle S^2 \rangle^{1/2}$ and hydrodynamic radius R_H of the micelles as functions of M_w were found to be also well described by the corresponding theories for the wormlike spherocylinder or wormlike chain models. The micelles grow in size with increasing T to greater length for longer hydrophobic chain, *i.e.*, alkyl group of the surfactants. They were rather flexible compared to the micelles formed with other polyoxyethylen alkyl ethers. The cross-sectional diameter d and spacings s between adjacent hexaoxyethylene chains on the micellar surface were similar in the $C_{16}E_7$ and $C_{18}E_7$ micelles. [DOI 10.1295/polymj.37.368]

KEY WORDS Polyoxyethylene Alkyl Ether / Micelle / Light Scattering / Diffusion Coefficient / Hydrodynamic Radius / Radius of Gyration / Wormlike Chain /

Nonionic surfactants polyoxyethylene mono-alkyl ether $H(CH_2)_i(OCH_2CH_2)_jOH$, hereafter abbreviated as C_iE_j, form polymerlike micelles in dilute aqueous solution (L_1 phase) below the lower consolute phase boundary. The micelles are known to grow in size with increasing surfactant concentration and raising temperature, in particular when approaching the phase boundary. The polymerlike micelles have certain similarities to real polymers and have been, thus, characterized with the use of experimental techniques employed in the polymer solution studies, such as static (SLS) and dynamic light scattering (DLS),[1–6,9] small-angle neutron scattering (SANS),[10–12] viscometry,[12,13] pulsed-field gradient NMR,[2–5] and so forth. However, the micelles possess the essential difference from polymers that the micellar size and its distribution, in general, depend on surfactant concentration, temperature, intermicellar thermodynamic interactions, and other factors. It is formidably difficult to achieve separate evaluation of the micellar growth and the enhancement of the intermicellar interactions as functions of surfactant concentration. Therefore, the interpretations given hitherto for the observed results especially by the SLS and DLS experiments are not unequivocal.

In the previous papers, we have studied $C_{12}E_6$ and $C_{14}E_6$ micelles,[14] $C_{14}E_8$, $C_{16}E_8$, and $C_{18}E_8$ micelles,[15] and $C_{10}E_5$ and $C_{10}E_6$ micelles,[16] in dilute aqueous solutions by SLS and DLS measurements. The SLS data have been analyzed by using the thermodynamic theory[17,18] of light scattering for micellar solutions to yield the molar mass M_w of the micelle as a function of surfactant concentration, along with values of the cross-sectional diameter d. The results of the hydrodynamic radius R_H and mean-square radius of gyration $\langle S^2 \rangle$ as functions of M_w have been found to be well described by the corresponding theory[19–22] with wormlike spherocylinder or chain model, providing the information of the micellar size, structure, and intrinsic flexibility.

In this work, we have applied the same method to micelles of heptaoxyethylene tetradecyl $C_{16}E_7$ and octadecyl $C_{18}E_7$ ethers, in order to investigate effects of the hydrophobic chain length of the surfactant molecules on the micellar characteristics.

EXPERIMENTAL

Materials

High-purity $C_{16}E_7$ and $C_{18}E_7$ samples were purchased from Nikko Chemicals Co. Ltd. and used without further purification. The solvent water used was high purity (ultrapure) water prepared with Simpli Lab water purification system of Millipore Co.

Phase Diagram

Cloud-point temperatures of given test solutions

†To whom correspondence should be addressed (E-mail: einaga@cc.nara-wu.ac.jp).

were determined as the temperatures at which intensity of the laser light transmitted through the solution abruptly decreased when temperature was gradually raised, by the fact that the originally transparent solutions became turbid.

Static Light Scattering

SLS measurements were performed to obtain the weight-average molar mass M_w of the $C_{16}E_7$ and $C_{18}E_7$ micelles. The scattering intensities were measured for each solution and for the solvent water at scattering angles θ ranging from 30 to 150° and at temperatures T ranging from 30.0 to 45.0 °C for $C_{16}E_7$ solutions and from 38.0 to 44.0 °C for $C_{18}E_7$ solutions. The ratio $Kc/\Delta R_\theta$ was obtained for each solution as a function of θ and extrapolated to zero scattering angle to evaluate $Kc/\Delta R_0$. Here, c is the surfactant mass concentration, ΔR_θ is the excess Rayleigh ratio at θ, and K is the optical constant defined as

$$K = \frac{4\pi^2 n^2 (\partial n/\partial c)_{T,p}^2}{N_A \lambda_0^4} \tag{1}$$

with N_A being the Avogadro's number, λ_0 the wavelength of the incident light in vacuum, n the refractive index of the solution, $(\partial n/\partial c)_{T,p}$ the refractive index increment, T the absolute temperature and p the pressure. The plot of $Kc/\Delta R_\theta$ *vs.* $\sin^2(\theta/2)$ affords a good straight line for all the micelle solutions studied. The apparent mean-square radius of gyration of the micelles was determined from the slope of the straight line as described below.

The apparatus used is an ALV DLS/SLS-5000/E light scattering photogoniometer and correlator system with vertically polarized incident light of 632.8 nm wavelength from a Uniphase Model 1145P He–Ne gas laser. For a calibration of the apparatus, the intensity of light scattered from pure benzene was measured at 25.0 °C at a scattering angle of 90°, where the Rayleigh ratio $R_{Uv}(90)$ of pure benzene for unpolarized scattered light with polarized incident light at a wavelength of 632.8 nm was taken as 11.84×10^{-6} cm^{-1}.[23,24]

The micellar solutions were prepared by dissolving appropriate amount of the surfactant in water. Complete mixing and micelle formation were achieved by stirring using a magnetic stirrer at least for one day. The solutions thus prepared were optically purified by filtration through a membrane of 0.20 μm pore size and transferred into optically clean NMR tubes of 10 mm diameter which was used as scatterring cells. The weight concentrations w of test solutions were determined gravimetrically and converted to mass concentrations c by the use of the densities ρ of the solutions given below.

The refractive index increment $(\partial n/\partial c)_{T,p}$ was measured at 25.0, 35.0, and 45.0 °C for $C_{16}E_7$ micelle solutions, and at 38.0, 42.0, and 46.0 °C for $C_{18}E_8$ micelle solutions, at 632.8 nm with a Union Giken R601 differential refractometer. The results were 0.1314 cm^3/g for $C_{16}E_7$ solutions and 0.1116 cm^3/g for $C_{18}E_7$ solutions, irrespective of temperature.

Dynamic Light Scattering

DLS measurements were carried out to determine the translational diffusion coefficient D for the micelles in water at various temperatures in the one phase (L_1 phase) region below or between the phase separation boundaries shown below by the use of the same apparatus and light source as used in the SLS studies described above. The normalized autocorrelation function $g^{(2)}(t)$ of scattered light intensity $I(t)$, *i.e.*,

$$g^{(2)}(t) = \frac{\langle I(0)I(t)\rangle}{\langle I(0)\rangle^2} \tag{2}$$

was measured at scattering angles θ ranging from 30 to 150°.

All the test solutions studied are the same as those used in the SLS studies. From the data for $g^{(2)}(t)$, we determined D by the equation

$$(1/2)\ln[g^{(2)}(t) - 1] = (1/2)\ln f - K_1 t + \cdots \tag{3}$$

$$D = \lim_{q \to 0} K_1/q^2 \tag{4}$$

Here, f is the coherent factor fixed by the optical system, K_1 is the first cumulant, and q is the magnitude of the scattering vector defined as

$$q = \frac{4\pi n}{\lambda_0} \sin(\theta/2) \tag{5}$$

It should be noted that the D values should be regarded as the z-average, since the micelles observed may have distribution in size.

Density

The solution density ρ required for the calculation of c and the partial specific volume v was measured at 25.0, 35.0, and 45.0 °C for $C_{16}E_7$ micelle solutions, and at 38.0, 42.0, and 46.0 °C for $C_{18}E_7$ micelle solutions with a pycnometer of the Lipkin–Davison type. For both $C_{16}E_7$ and $C_{18}E_7$ micelle solutions, ρ was independent of w. Thus, we have used literature values of the density ρ_0 of pure water at corresponding temperatures for ρ, and the v values of the micelles have been calculated as ρ_0^{-1}.

RESULTS AND DISCUSSION

Phase Behavior

Figure 1 depicts phase diagrams of the $C_{16}E_7$ +

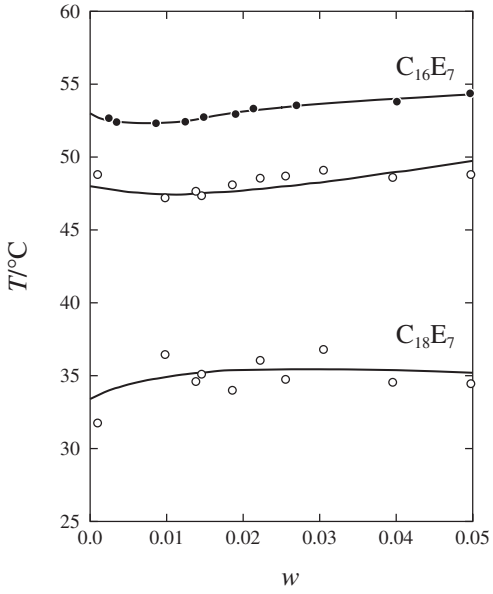

Figure 1. Cloud Point Curves of the $C_{16}E_7$ + water (filled circles) and $C_{18}E_7$ + water (unfilled circles) systems.

water (filled circles) and $C_{18}E_7$ + water (unfilled circles) systems. The cloud point curves for both the $C_{16}E_7$ and $C_{18}E_7$ micelle solutions represent phase separation boundaries of the LCST (lower critical solution temperature) type, above which the solutions phase-separate into two phases. The LCST of the former system is higher by about 5 °C than that of the latter. The $C_{18}E_7$ + water system has another phase boundary of the UCST (upper critical solution temperature) type in addition to that of the LCST type. Thus, the $C_{18}E_7$ micelles are stable only in the limitted temperature range in between the two phase boundaries.

Static Light Scattering

$Kc/\Delta R_0$ for all the solutions of the $C_{16}E_7$ and $C_{18}E_7$ micelles at various temperatures are plotted against c in Figures 2 and 3, respectively. The data points at fixed T follow a curve convex downward whose curvature becomes slightly less significant as T is increased. The $Kc/\Delta R_0$ value at fixed c decreases with increasing T.

As mentioned in the Introduction, we have analyzed the present SLS data by employing a light-scattering theory for micellar solutions formulated by Sato[17] with wormlike spherocylinder model for polymerlike micelles, in order to determine the M_w values of the micelles at finite concentrations c. The model consists of a wormlike cylinder of contour length $L - d$ with cross-sectional diameter d and two hemispheres of diameter d which cap both ends of the cylinder. Stiffness of the wormlike cylinder is represented by the stiffness parameter λ^{-1}. Sato has dealt with multiple equilibrium between micelles of different sizes and

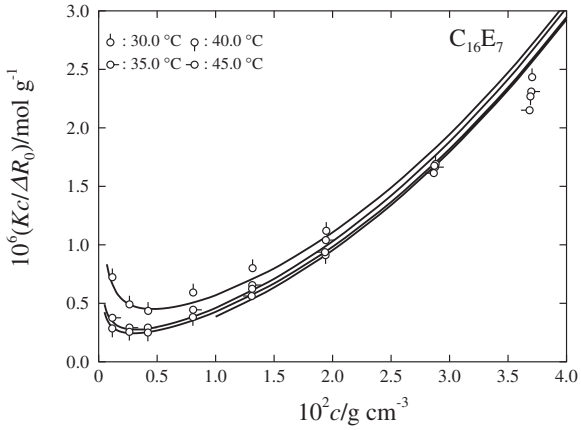

Figure 2. Plots of $(Kc/\Delta R_0)$ against c for the $C_{16}E_7$ micelle solutions at various T indicated.

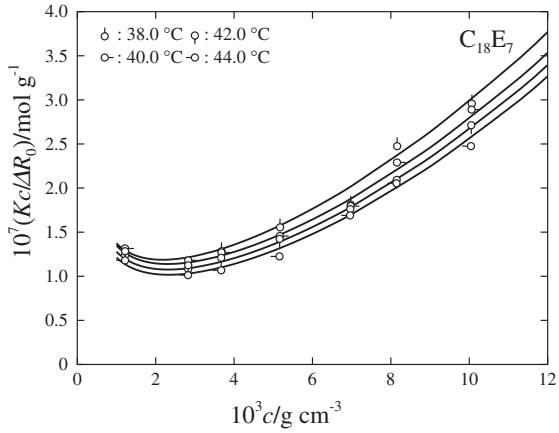

Figure 3. Plots of $(Kc/\Delta R_0)$ against c for the $C_{18}E_7$ micelle solutions at various T indicated.

monomer, by representing chemical potentials of the micelles as functions of c with the free energy parameter g_2 which controls micellar formation and growth, and the strength $\hat{\epsilon}$ of the attractive interactions between spherocylindrical micelles, in a similar way to the classical mean-field and recent molecular theoretical approaches.[25–27] As a result, the number-N_n and weight-average aggregation number N_w of the micelles have been formulated as functions of c along with the micellar size distribution functions. Then, he has derived the equation for light scattering of micelle solutions by using the chemical potentials. The result for $Kc/\Delta R_0$ reads

$$\frac{Kc}{\Delta R_0} = \frac{1}{M_w(c)} + 2A(c)c \tag{6}$$

where $M_w(c)$ is the weight-average molar mass of the micelles and $A(c)$ is the apparent second virial coefficient in a sense that it is comprised of the second, third, and the higher virial coefficient terms. Both are functions of c, containing three parameters d, g_2, and $\hat{\epsilon}$. We refer the expressions for the functions

$M_w(c)$ and $A(c)$ to the original papers[17,18] or our previous paper,[14] since they are fairly involved.

In Figures 4 and 5 are demonstrated the results of curve-fitting of the theoretical calculations to the experimental values of $Kc/\Delta R_0$ for the $C_{16}E_7$ and $C_{18}E_7$ micelle solutions, respectively. Here, the solid curves represent the best-fit theoretical values calculated by eq 6 by choosing the proper values of d, g_2, and $\hat{\epsilon}$. It is seen that the solid curves are in good coincidence with the respective data points at given temperatures. The agreement between the calculated and observed results implies that the $C_{16}E_7$ and $C_{18}E_7$ micelles in dilute aqueous solutions are represented by the wormlike spherocylinder model. From the curve fitting, we

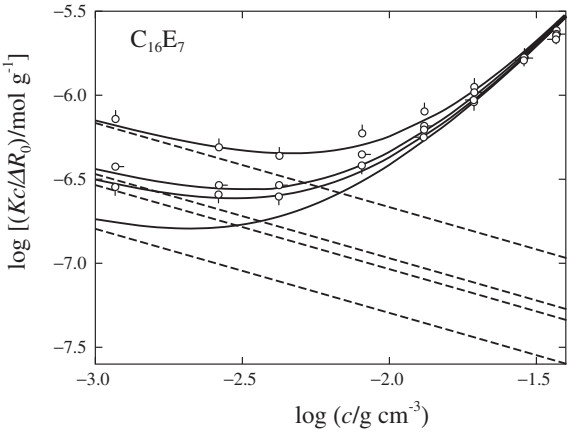

Figure 4. The results of the curve fitting for the plots of $Kc/\Delta R_0$ against c for the $C_{16}E_7$ micelle solutions at various T: Symbols have the same meaning as those in Figure 2. The solid and dashed curves represent $Kc/\Delta R_0$ and $1/M_w(c)$, respectively. Temperatures T are 30.0, 35.0, 40.0, and 45.0 °C from top to bottom, respectively.

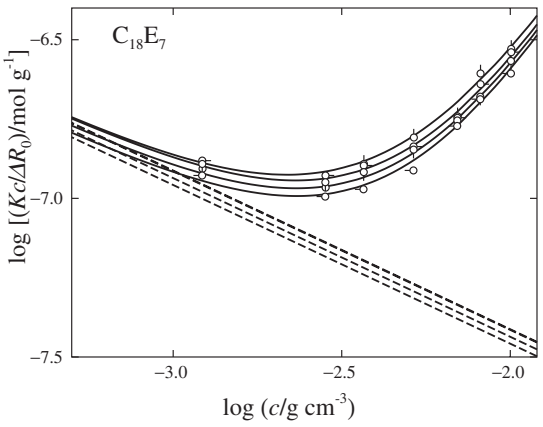

Figure 5. The results of the curve fitting for the plots of $Kc/\Delta R_0$ against c for the $C_{18}E_7$ micelle solutions at various T: Symbols have the same meaning as those in Figure 3. The solid and dashed curves represent $Kc/\Delta R_0$ and $1/M_w(c)$, respectively. Temperatures T are 38.0, 40.0, 42.0, and 44.0 °C from top to bottom, respectively.

have determined the M_w values of each micelles as a function of c. The dashed lines represent the values of $1/M_w(c)$ at respective temperatures. For all the micelles at any fixed T, they have a slope of -0.5, showing that M_w increases with c as $M_w \propto c^{1/2}$ in the range of c examined, as in the case of the previous findings for the $C_{12}E_6$ and $C_{14}E_6$ micelles,[14] $C_{14}E_8$, $C_{16}E_8$, and $C_{18}E_8$ micelles,[15] and $C_{10}E_5$ and $C_{10}E_6$ micelles.[16] These results are in good correspondence with simple theoretical predictions derived from the thermodynamic treatments of multiple equilibria among micelles of various aggregation numbers.[17,25–27] The solid and dashed curves tend to coincide with each other at small c and the difference between them steadily increases with increasing c. The results indicate that contributions of the virial coefficient terms to $Kc/\Delta R_0$ are small at small c but progressively increase with increasing c as expected.

The d value chosen in the curve-fitting procedure is 2.5 nm for both $C_{16}E_7$ and $C_{18}E_7$ micelles at any T studied. The values of g_2 and $\hat{\epsilon}$ determined are plotted against T in Figures 6 and 7, respectively. It is found that when compared at fixed T, the g_2 value is larger in the $C_{18}E_7$ micelles than in the $C_{16}E_7$ micelles. For each micelle, g_2 is an increasing function of T, though degree of the increase is small in the former micelles. These results for g_2 may reflect the fact that alkyl group of the surfactant molecules is longer in $C_{18}E_7$ than in $C_{16}E_7$ but the length of oxyethylene group is the same for both the surfactant. The values of $\hat{\epsilon}$ for the $C_{18}E_7$ micelle solutions are larger than those for the $C_{16}E_7$ micelle solutions, although the differences are rather small.

Molar Mass Dependence of Radius of Gyration

We have determined the apparent mean-square radius of gyration $\langle S^2 \rangle_{app}$ for the $C_{16}E_7$ and $C_{18}E_7$ micelles from the slope of the $Kc/\Delta R_\theta$ *vs.* $\sin^2(\theta/2)$

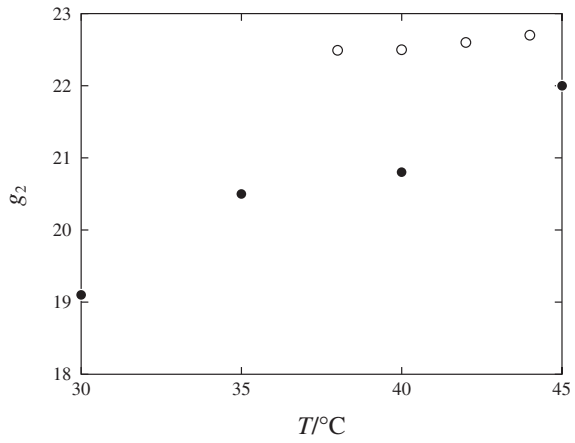

Figure 6. Temperature dependence of g_2 for the $C_{16}E_7$ + water (filled circles) and $C_{18}E_7$ + water (unfilled circles) systems.

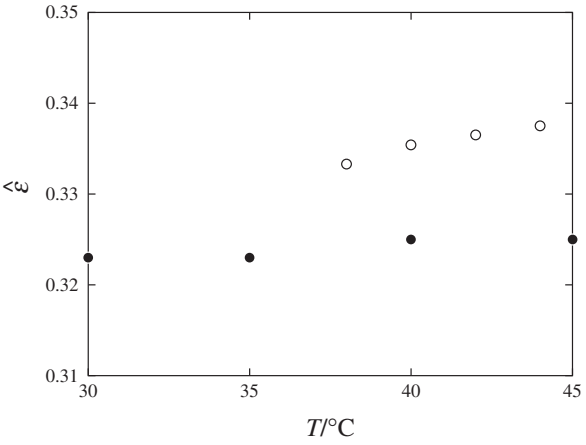

Figure 7. Temperature dependence of $\hat{\epsilon}$ for the $C_{16}E_7$ + water (filled circles) and $C_{18}E_7$ + water (unfilled circles) systems.

plot, on the basis of the fundamental light scattering equation

$$\frac{Kc}{\Delta R_\theta} = \frac{1}{M_w(c)}\left(1 + \frac{1}{3}\langle S^2\rangle q^2\right) + 2A_2c + \cdots \quad (7)$$

at finite concentrations by using the $M_w(c)$ values determined as described above. Here, A_2 is the second virial coefficient and $\langle S^2\rangle$ is denoted by $\langle S^2\rangle_{app}$, since it may possibly be affected by intermicellar interactions and then concentration-dependent. Molar mass M_w dependence of $\langle S^2\rangle_{app}^{1/2}$ is exhibited in Figures 8 and 9 for the $C_{16}E_7$ and $C_{18}E_7$ micelles, respectively, at various T indicated. All the data points for each micelle form a single composite curve irrespective of temperature and concentration, implying that the values of $\langle S^2\rangle_{app}^{1/2}$ determined at finite c correspond to those for the individual micelles free from inter- and intra-micellar interactions or excluded volume effects. The solid curves show the best-fit theoretical values of $\langle S^2\rangle$ for the wormlike chain model calculated by[22]

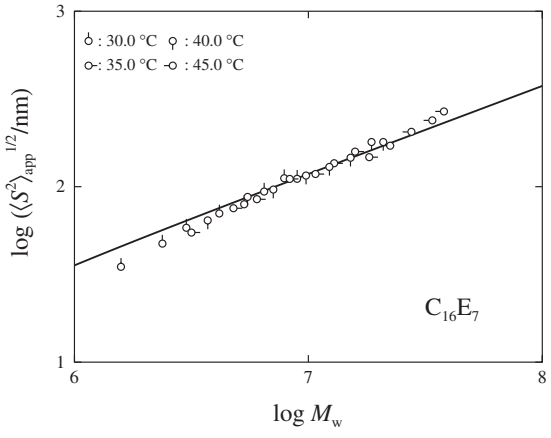

Figure 8. Double-logarithmic plots of $\langle S^2\rangle_{app}^{1/2}$ against M_w for the $C_{16}E_7$ micelles at various T indicated. The solid curve represents the theoretical values calculated by eqs 8 and 9.

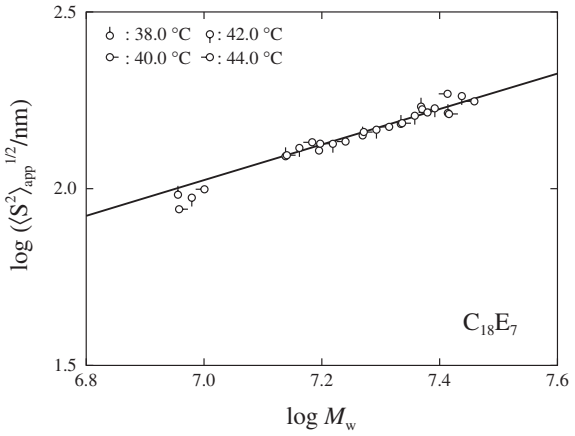

Figure 9. Double-logarithmic plots of $\langle S^2\rangle_{app}^{1/2}$ against M_w for the $C_{18}E_7$ micelles at various T indicated. The solid curve represents the theoretical values calculated by eqs 8 and 9.

$$\lambda^2\langle S^2\rangle = \frac{\lambda L}{6} - \frac{1}{4} + \frac{1}{4\lambda L} - \frac{1}{8\lambda^2L^2}(1 - e^{-2\lambda L}) \quad (8)$$

Here, the values of L_w calculated by

$$L_w = \frac{4\nu M_w}{\pi N_A d^2} + \frac{d}{3} \quad (9)$$

were used in place of L in eq 8.

In the calculation, the d value 2.5 nm obtained in the preceding section was used and then the value of λ^{-1} was determined as 25.0 nm for the $C_{16}E_7$ micelles and 22.0 nm for the $C_{18}E_7$ micelles to achieve the best-fit to the observed results. It is found that the calculated results well explains the observed behavior of $\langle S^2\rangle_{app}^{1/2}$, although the theoretical curves deviate upward from the observed values at small M_w especially for the $C_{16}E_7$ micelles for the reason that cannot be specified at present. The agreement again shows that the $C_{16}E_7$ and $C_{18}E_7$ micelles assume a wormlike shape in dilute aqueous solution.

Hydrodynamic Radius of the Micelle

From the mutual diffusion coefficient D determined from DLS results by eq 4, the apparent hydrodynamic radius $R_{H,app}$ as a function of c has been evaluated by[14,28,29]

$$D = \frac{(1 - \nu c)^2 M}{6\pi\eta_0 N_A R_{H,app}}\left(\frac{\partial\pi}{\partial c}\right)_{T,p} \quad (10)$$

where M is the molar mass of the solute, η_0 is the solvent viscosity, and $(\partial\pi/\partial c)_{T,p}$ is the osmotic compressibility. In this evaluation, we have used the SLS data for $(\partial\pi/\partial c)_{T,p}$ together with the values of $M_w(c)$ obtained in the previous section in place of M. The values of $R_{H,app}$ thus determined at various T are plotted against c in Figures 10 and 11 for the $C_{16}E_7$ and $C_{18}E_7$ micelles, respectively. It was found that at any given T, $R_{H,app}$ increases with increasing c. It

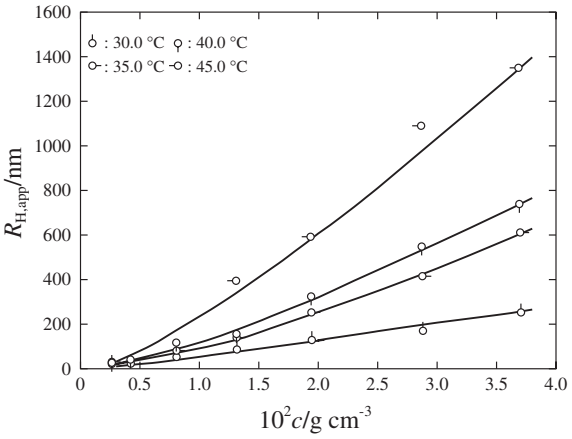

Figure 10. Concentration dependence of $R_{H,app}$ for the $C_{16}E_7$ micelles at indicated T.

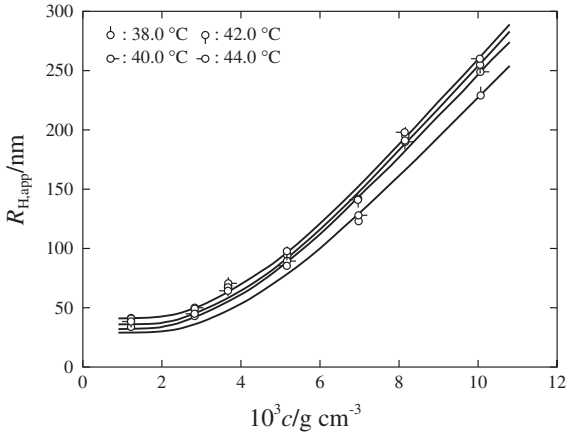

Figure 11. Concentration dependence of $R_{H,app}$ for the $C_{18}E_7$ micelles at indicated T.

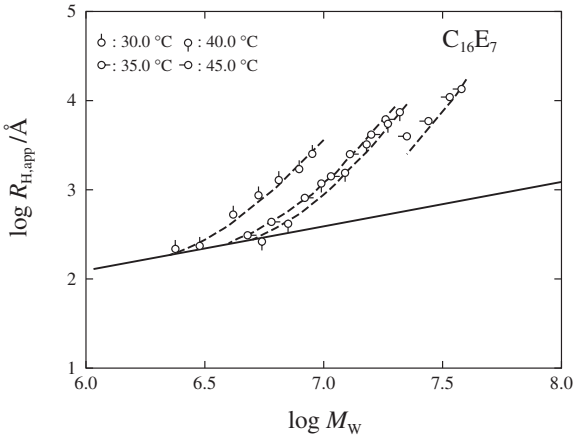

Figure 12. Double-logarithmic plots of $R_{H,app}$ against M_w for the $C_{16}E_7$ micelles at various T indicated. The solid curve represents the theoretical values calculated by eqs 9 and 11.

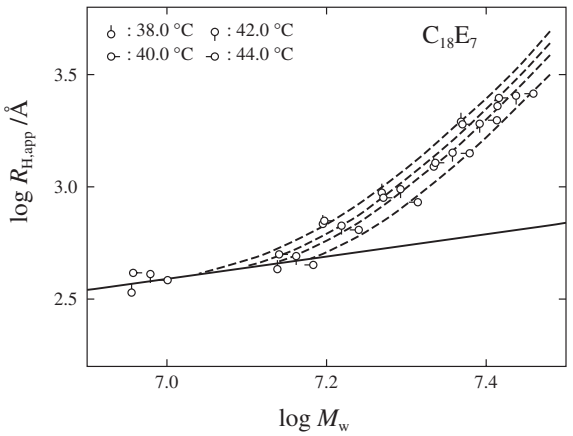

Figure 13. Double-logarithmic plots of $R_{H,app}$ against M_w for the $C_{18}E_7$ micelles at various T indicated. The solid curve represents the theoretical values calculated by eqs 9 and 11.

should be noted that the $R_{H,app}$ values do not necessarily correspond to those for "isolated" micelles. The increase of $R_{H,app}$ may reflect two effects; micellar growth in size and enhancement of the effects of the intermicellar hydrodynamic interactions with increasing c.

In Figures 12 and 13, $R_{H,app}$ are double-logarithmically plotted against M_w for $C_{16}E_7$ and $C_{18}E_7$ micelles, respectively. In our previous papers,[14–16] it has been shown that in similar plots, the data points at different T asymptotically form a single composite curve at small M_w, or at small c, suggesting that the effects of the intermicellar hydrodynamic interactions on $R_{H,app}$ become less significant as c is lowered and are negligible in the asymptotic region of low c. The present results are similar to the previous findings. Thus, we analyze the data points at small M_w at each fixed T in Figures 12 and 13 by regarding them to give the relationship between R_H and M_w for the "isolated" micelles.

The translational diffusion coefficient D is formulated by Norisuye *et al.*[19] for the wormlike spherocylinder model and by Yamakawa *et al.*[20,21] for the wormlike cylinder model, as a function of L with including the parameters d and λ^{-1}. From these theories, we may derive the expression for R_H as a function of L, d, and λ^{-1} over the entire range of L including the sphere, *i.e.*, the case $L = d$. It reads

$$R_H = \frac{L}{2f(\lambda L, \lambda d)} \tag{11}$$

The expression for the function f is so lengthy that we refer it to the original papers.[19–21] By eqs 9 and 11, the theoretical values of R_H have been calculated as a function of M_w for various values of λ^{-1} with the use of the d values 2.5 nm determined above for the $C_{16}E_7$ and $C_{18}E_7$ micelles. Here, the L_w values calculated by eq 9 were again used in place of L in eq 11. In Figures 12 and 13, the solid lines are best-fit curves to the data points for which the effects of the intermi-

cellar hydrodynamic interactions are considered to be negligible. We note that the data of $R_{H,app}$ for the $C_{16}E_7$ micelles at 45.0 °C are not avilable at small M_w or in other word at low c in Figure 12. It is found that the theoretical curves well describe the observed behavior of R_H as a function of M_w, implying that the micelles observed may be represented with the wormlike spherocylinder model. The data points at fixed T steeply increase with M_w deviating upward from the solid curve due to the enhancement of the intermicellar hydrodynamic interactions with increasing c.

The curve fittings yield a λ^{-1} value of 6.0 nm for both $C_{16}E_7$ and $C_{18}E_7$ micelles. These λ^{-1} values are considerably smaller than those obtained above from the analysis of $\langle S^2 \rangle$. These differences may be attributed to the fact that there is a distribution in micellar size and different averages are reflected in $\langle S^2 \rangle_{app}^{1/2}$ and R_H. It has been theoretically shown[17,27] that the highly extended micelles have the most probable distribution in size and the distribution affords a value *ca.* 2 as the ratio of the weight-average aggregation number N_w to the number-average N_n irrespective of T and c. It is anticipated that the ratio $N_w/N_n = 2$ is realized at the limit of extensive micellar growth, which can be ascertained by the setup of the relation $M_w \propto c^{1/2}$ as observed in Figures 4 and 5 in the present case. Thus, the micelles observed in this study are considered to have the most probable distribution in size and the distribution affects the evaluation of λ^{-1} from $\langle S^2 \rangle^{1/2}$ and R_H.

The λ^{-1} value from R_H indicate that the present micelles of $C_{16}E_7$ and $C_{18}E_7$ are rather flexible compared to the micelles of other C_iE_j molecules studied previously.[14–16]

Micelle Structure

Figure 14 shows concentration dependence of L_w for each of the micelles at a few or several temperatures examined in this study. The weight-average contour length L_w was calculated by eq 9 from the values of $M_w(c)$ and d obtained above. For each micelle, L_w becomes larger as c is increased or T is raised. It is found that the micelles grow to a greater length as longer the alkyl chain length of the surfactant molecules. This result may come from the thermodynamic reason that attractive interactions among $C_{18}E_7$ molecules are stronger than among $C_{16}E_7$ molecules as demonstrated above by the values of g_2 (see Figure 6).

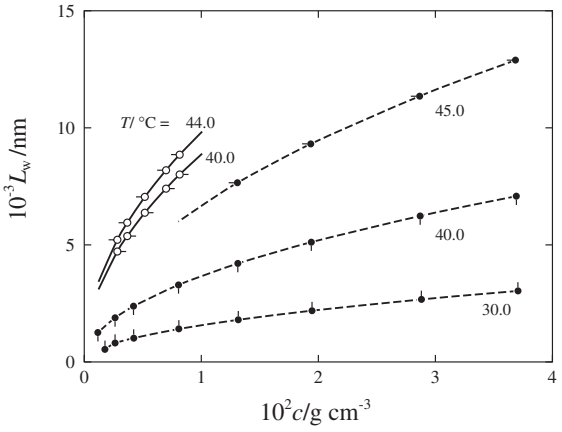

Figure 14. Concentration dependence of L_w for the $C_{16}E_7$ (filled circles) and $C_{18}E_7$ (unfilled circles) micelles at various T indicated.

The spacings s between the hydrophilic tails of adjacent surfactant molecules on the micellar surface are evaluated from the values of d, L_w, and the aggregation number N_w calculated from M_w. The s value obtained is *ca.* 1.37 nm for the $C_{16}E_7$ micelles and *ca.* 1.41 nm for the $C_{18}E_7$ micelles irrespective of c and T. The result indicates that the micelles are formed and grow in the way that the hydrophilic groups of the C_iE_7 molecules are located at intervals of these s values on the micellar surface on the average. These s values are not significantly different from each other, presumably reflecting that the hydrophilic groups are the same in the two surfactants.

CONCLUSIONS

In the present work, we have determined shape, size, and flexibility of the $C_{16}E_7$ and $C_{18}E_7$ micelles at finite surfactant concentrations c from SLS and DLS experiments by employing the same method as used in the previous study for the C_iE_j micelles.[14–16] The results of $Kc/\Delta R_0$ from SLS have been analyzed with the aid of the thermodynamic theory[17] for light scattering of micelle solutions formulated with wormlike spherocylinder model. The analyses have yielded the molar mass $M_w(c)$ as a function of c and the cross-sectional diameter d. The good agreement between the calculated and observed $Kc/\Delta R_0$ as a function of c indicates that the present micelles assume a shape of wormlike spherocylinders in dilute solutions.

The mean-square radius of gyration $\langle S^2 \rangle$ and the hydrodynamic radius R_H of the individual "isolated" micelles as functions of M_w ($\equiv M_w(c)$) have been successfully described by the corresponding theories for the wormlike chain and the wormlike spherocylinder models, respectively. The values of the stiffness parameter λ^{-1} evaluated from the fitting of the calculated values for $\langle S^2 \rangle$ or R_H to the experimental results have revealed that the micelles are far from rigid rods but rather flexible.

It has been found that the $C_{18}E_7$ micelles grow in length to a greater extent than the $C_{16}E_7$ micelles. The finding may imply that attractive interactions among surfactant molecules, by which micelles are

formed, are stronger in the $C_{18}E_7$ micelles with longer hydrophobic chain of alkyl group, as clearly evidenced by the large differences in the free energy parameter g_2. On the other hand, the cross-sectional diameter d of the cylindrical micelles and the spacings s of the adjacent hydrophilic chains on the micellar surface have been found to have approximately the same values for the $C_{16}E_7$ and $C_{18}E_7$ micelles.

Acknowledgment. The authors are grateful to Prof. Takahiro Sato at Osaka University, Japan and also to members of the NKO Academy for valuable discussions and comments.

REFERENCES

1. A. Bernheim-Groswasser, E. Wachtel, and Y. Talmon, *Langmuir*, **16**, 4131 (2000).
2. W. Brown, R. Johnson, P. Stilbs, and B. Lindman, *J. Phys. Chem.*, **87**, 4548 (1983).
3. T. Kato and T. Seimiya, *J. Phys. Chem.*, **90**, 1986 (1986).
4. W. Brown and R. Rymden, *J. Phys. Chem.*, **91**, 3565 (1987).
5. W. Brown, Z. Pu, and R. Rymden, *J. Phys. Chem.*, **92**, 6086 (1988).
6. T. Imae, *J. Phys. Chem.*, **92**, 5721 (1988).
7. W. Richtering, W. Burchard, and H. Finkelmann, *J. Phys. Chem.*, **92**, 6032 (1988).
8. T. Kato, S. Anzai, and T. Seimiya, *J. Phys. Chem.*, **94**, 7255 (1990).
9. H. Strunk, P. Lang, and G. H. Findenegg, *J. Phys. Chem.*, **98**, 11557 (1994).
10. P. Schurtenberger, C. Cavaco, F. Tiberg, and O. Regev, *Langmuir*, **12**, 2894 (1996).
11. G. Jerke, J. S. Pedersen, S. U. Egelhaaf, and P. Schurtenberger, *Langmuir*, **14**, 6013 (1998).
12. O. Glatter, G. Fritz, H. Lindner, J. Brunner-Papela, R. Mittelbach, R. Strey, and S. U. Egelhaaf, *Langmuir*, **16**, 8692 (2000).
13. T. R. Carale and D. Blankschtein, *J. Phys. Chem.*, **96**, 455 (1992).
14. S. Yoshimura, S. Shirai, and Y. Einaga, *J. Phys. Chem. B*, **108**, 15477 (2004).
15. N. Hamada and Y. Einaga, *J. Phys. Chem. B*, in press.
16. K. Imanishi and Y. Einaga, *J. Phys. Chem. B*, in press.
17. T. Sato, *Langmuir*, **20**, 1095 (2004).
18. R. Koyama and T. Sato, *Macromolecules*, **35**, 2235 (2002).
19. T. Norisuye, M. Motowoka, and H. Fujita, *Macromolecules*, **12**, 320 (1979).
20. H. Yamakawa and M. Fujii, *Macromolecules*, **6**, 407 (1973).
21. H. Yamakawa and T. Yoshizaki, *Macromolecules*, **12**, 32 (1979).
22. H. Benoit and P. Doty, *J. Phys. Chem.*, **57**, 958 (1953).
23. E. R. Pike, R. W. Pomeroy, and J. M. Vaughan, *J. Chem. Phys.*, **62**, 3188 (1975).
24. Y. Einaga, T. Mitani, J. Hashizume, and H. Fujita, *Polym. J.*, **11**, 565 (1979).
25. D. Blankschtein, G. M. Thurston, and G. B. Benedek, *J. Chem. Phys.*, **85**, 7268 (1986).
26. M. E. Cates and S. J. Candou, *J. Phys.: Condens. Matter*, **2**, 6869 (1990).
27. N. Zoeller, L. Lue, and D. Blankschtein, *Langmuir*, **13**, 5258 (1997).
28. B. J. Berne and R. Pecora, "Dynamic Light Scattering," John Wiley & Sons, New York, N.Y., 1976.
29. P. Stepanek, W. Brown, and S. Hvidt, *Macromolecules*, **29**, 8888 (1996).